Electronic Supplementary Material (ESI) for Catalysis Science & Technology.
This journal is © The Royal Society of Chemistry 2024

Selective Vapor-Phase Formation of Dimethylformamide via Oxidative Coupling of Methanol and Dimethylamine over Bimetallic Catalysts

SUPPORTING INFORMATION

Alexander P. Minne, Tristan Maxson, Tibor Szilvási, and James W. Harris*

Department of Chemical and Biological Engineering,

The University of Alabama, Tuscaloosa, AL, 35487

*Corresponding author: james.harris@eng.ua.edu

Table of Contents

S.1. Values of O_2 Adsorption and Dissociation on Single Crystal Surfaces

Table S.1. Values of O_2 adsorption and dissociation on pure Au surfaces.			
Facet	O_2 Adsorption Energy (kJ mol^{-1})	O_2 Dissociation Barrier (kJ mol^{-1})	Source
Au(111)	-7.72 [α]	132 [α]	[1]
Au(211)	-14.5 [α]	108 [α]	[2]
Au(321)	-16.4 [α]	96.5 [α]	[3]
AgAu(211)	Not Reported	21.2 [β]	[4]
Ag(111)	-38.6 [β]	34.7 [β]	[5]
Ag(110)	-38.6 [β]	32.8 [β]	[5]
Ag(100)	-65.6 [α]	Not Reported	[6]
Pd(111)	-87.8 [α]	68.5 [α]	[7]
Pd(110)	-125 [α]	16.4 [α]	[8]
Pd(100)	-73.3 [α]	11.6 [α]	[9]
[α] theory/calculated [β] experimental			

S.2. Process Flow Diagram

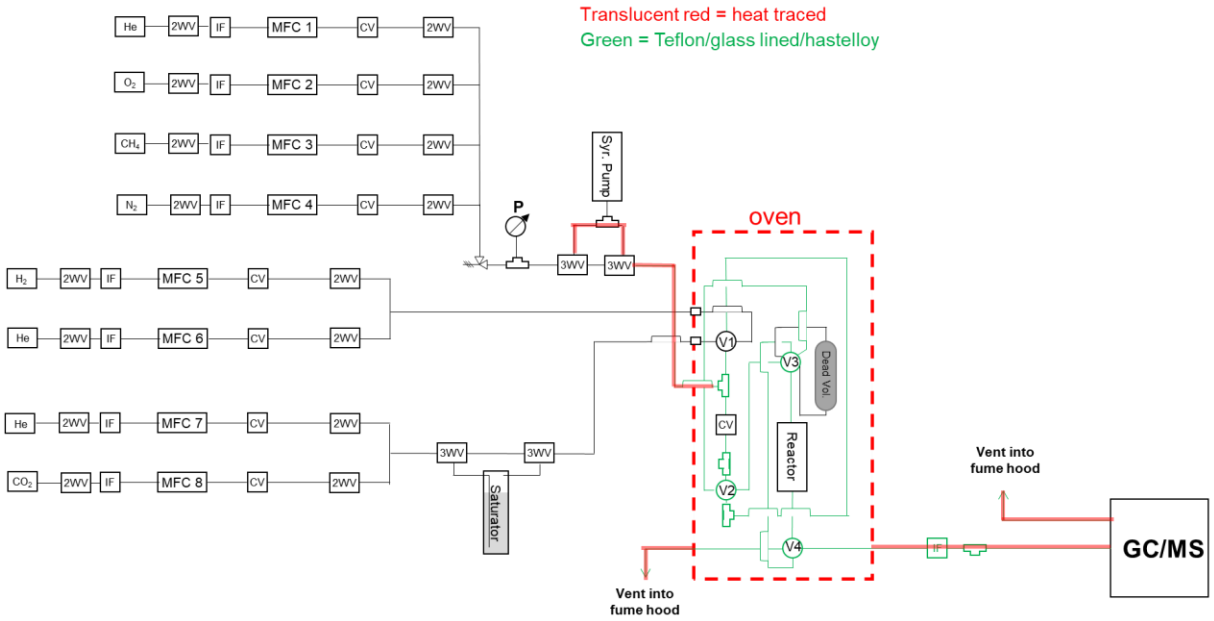

Figure S.1. Process flow diagram for the apparatus used for kinetic measurements.

S.3. Nitrogen Physisorption Isotherms

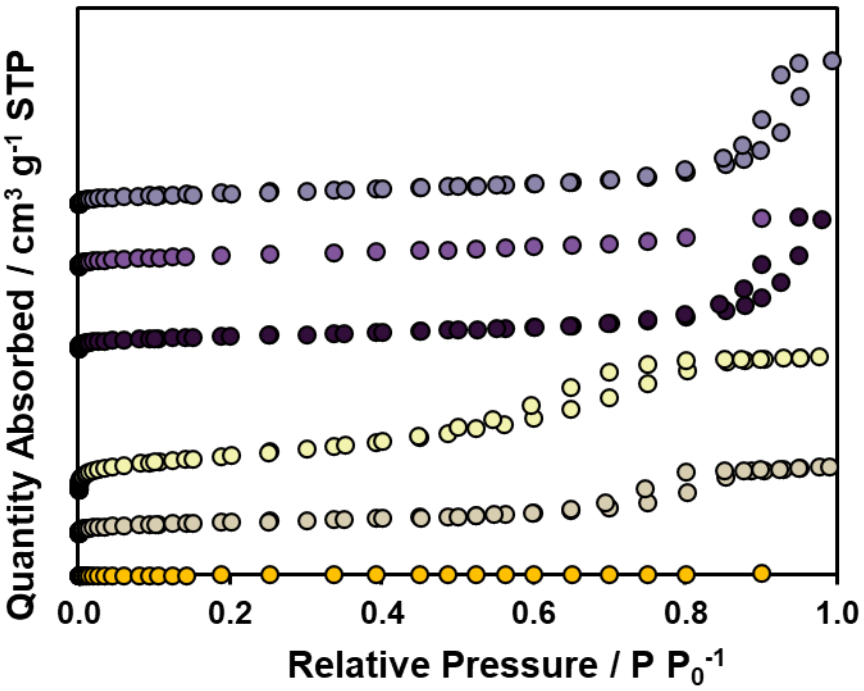

Figure S.2. N_2 physisorption isotherms for (top to bottom) 1:53 $PdAu/SiO_2$, 1:10 $PdAu/SiO_2$, 1:2 $PdAu/SiO_2$, Pd/SiO_2, 1:15 $AgAu/SiO_2$, and nanoporous gold.

S.4. SEM/TEM Images

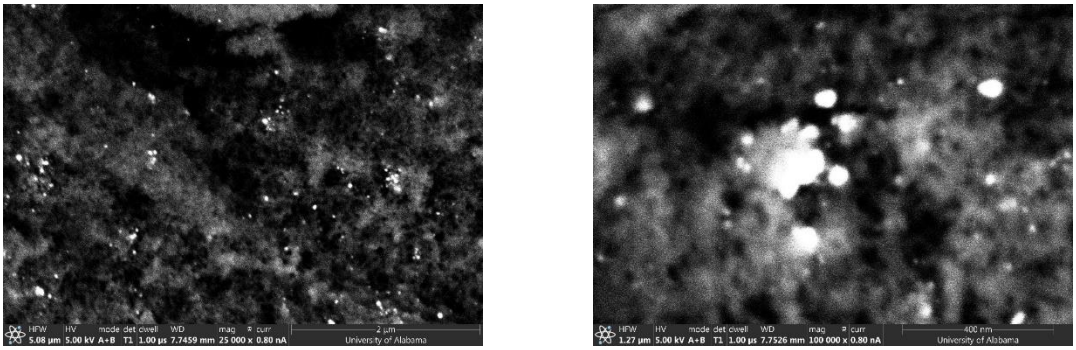

Figure S.3. SEM images of 1:2 PdAu/SiO_2.

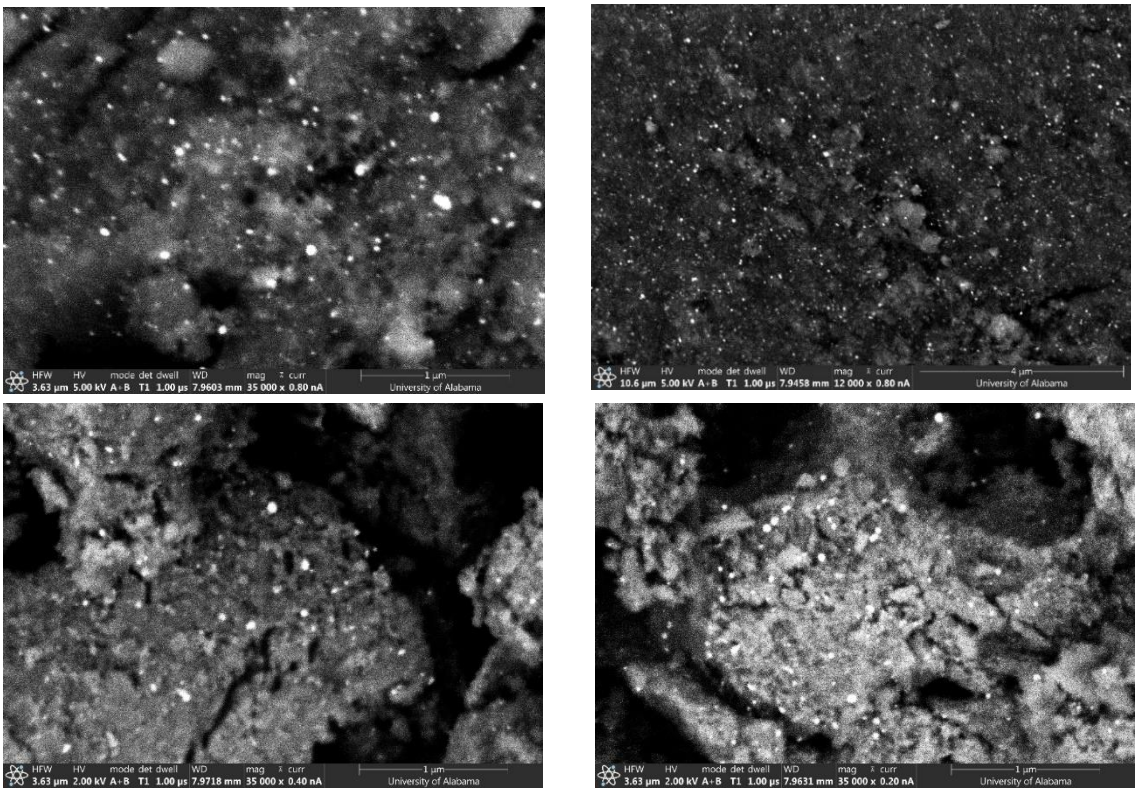

Figure S.4. SEM images of 1:15 AgAu/SiO_2.

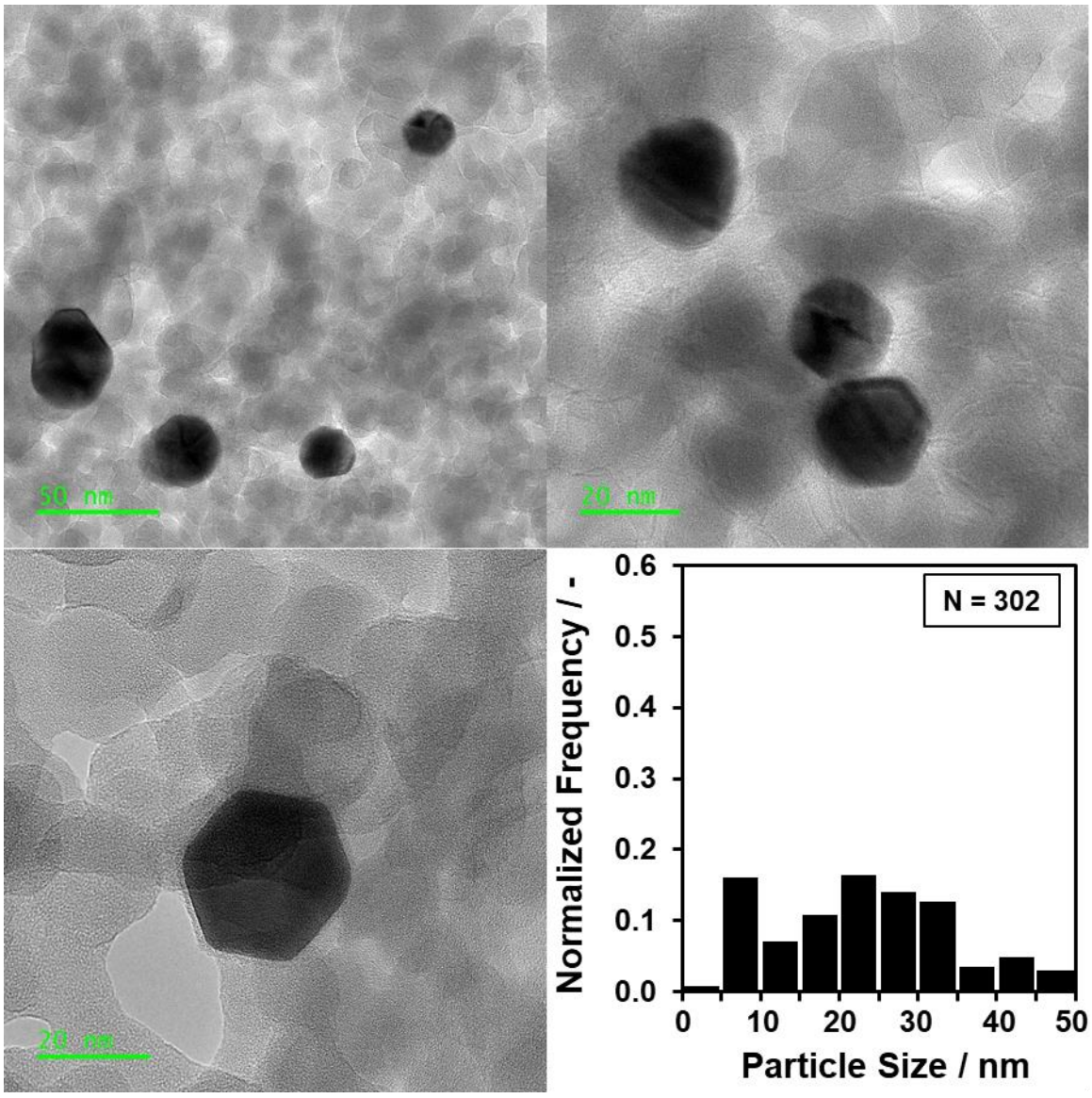

Figure S.5. TEM images and particle size distribution of 1:2 PdAu/SiO_2.

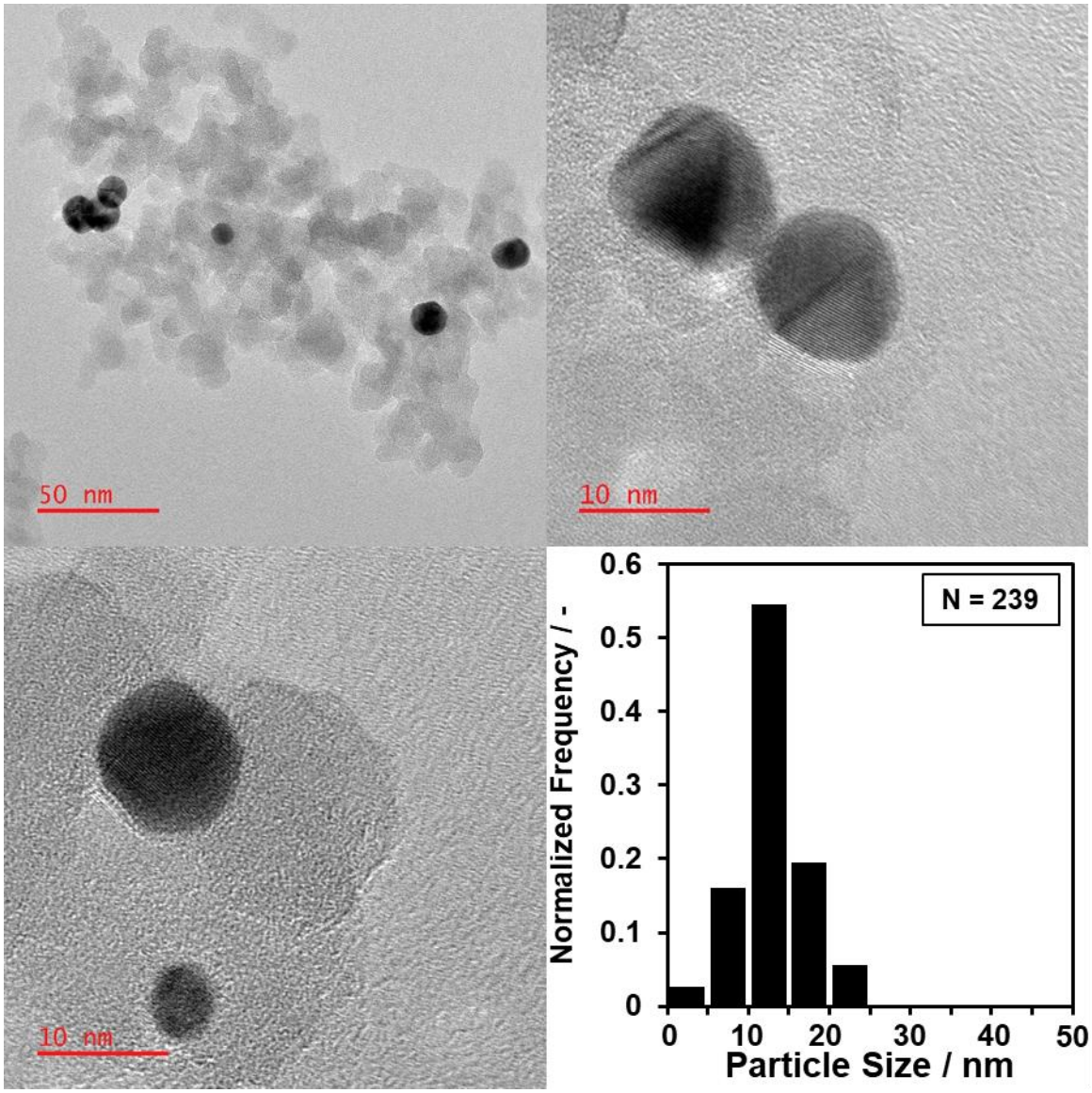

Figure S.6 TEM images and particle size distribution of 1:53 PdAu/SiO_2.

S.5 TEM Images of Used Catalyst Samples

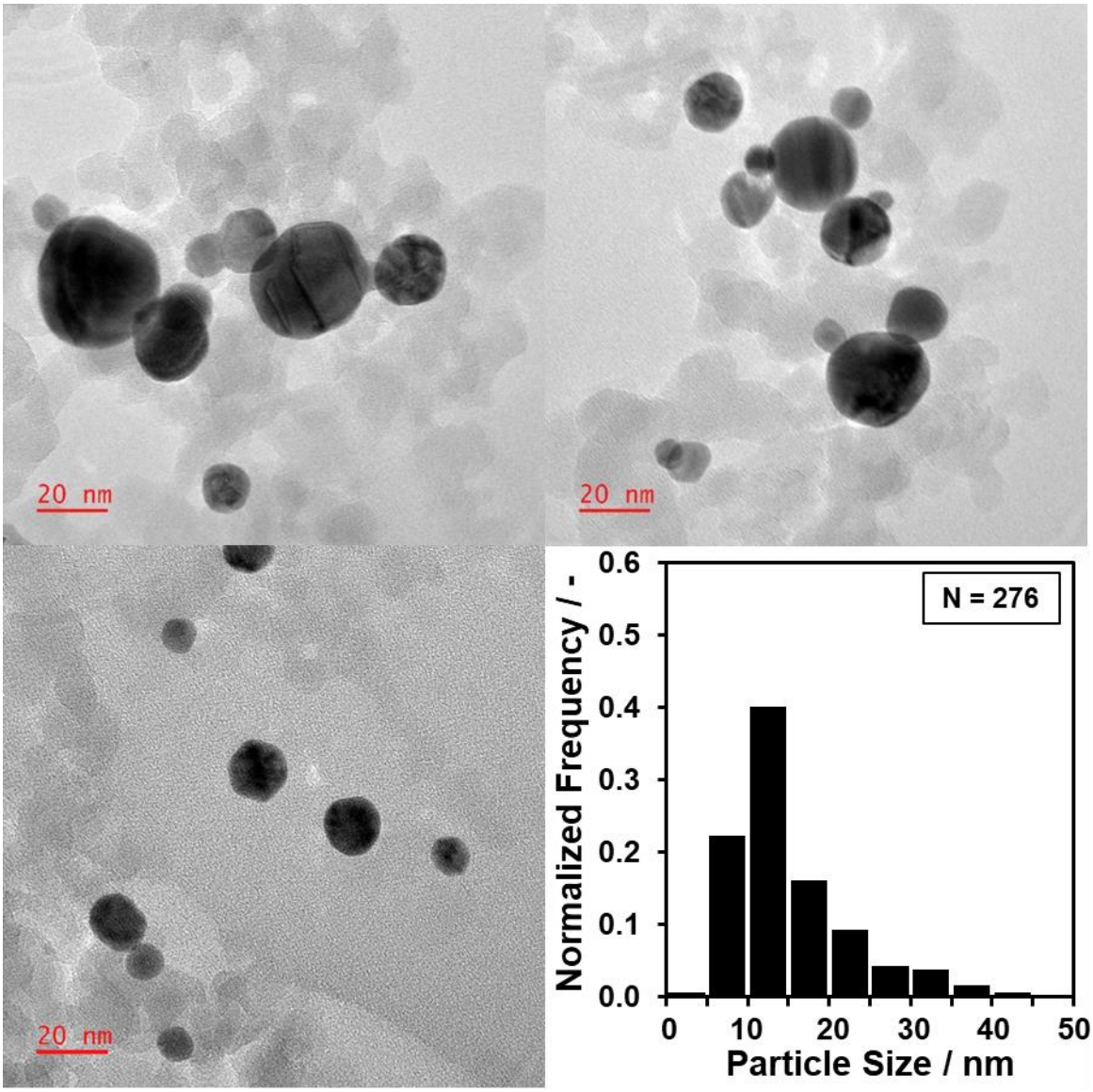

Figure S.7. TEM images and particle size distribution of used 1:10 PdAu/SiO_2. This particle sample was subjected to multiple kinetic experiments at various conditions, approximately 100 hours of time on stream. Average particle size was shown to be 15.3 ± 7.3 nm.

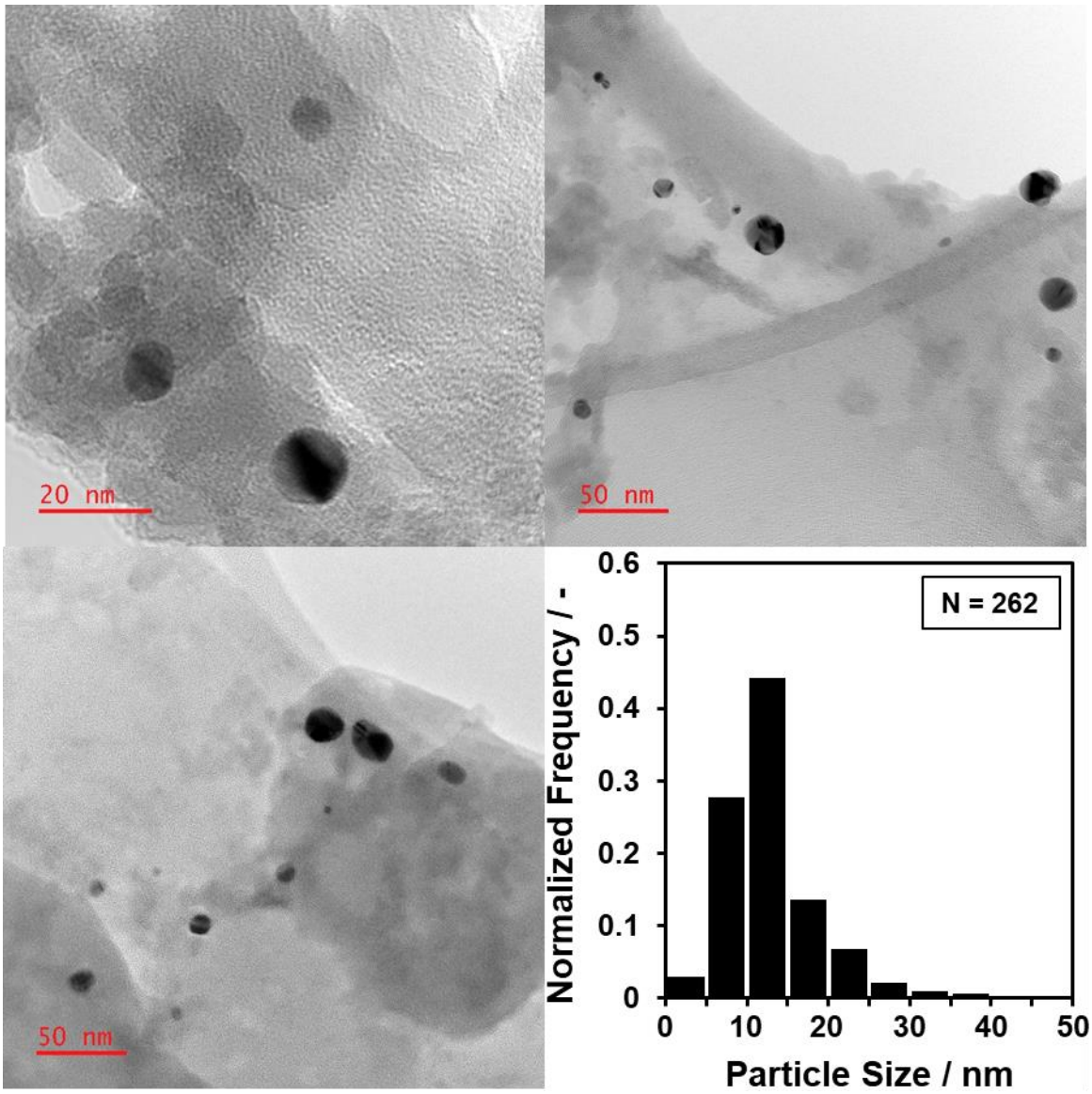

Figure S.8. TEM images and particle size distribution of used 1:15 AgAu/SiO_2. This particle sample was subjected to multiple kinetic experiments at various conditions, approximately 100 hours of time on stream. Average particle size was shown to be 13.0 ± 5.8 nm.

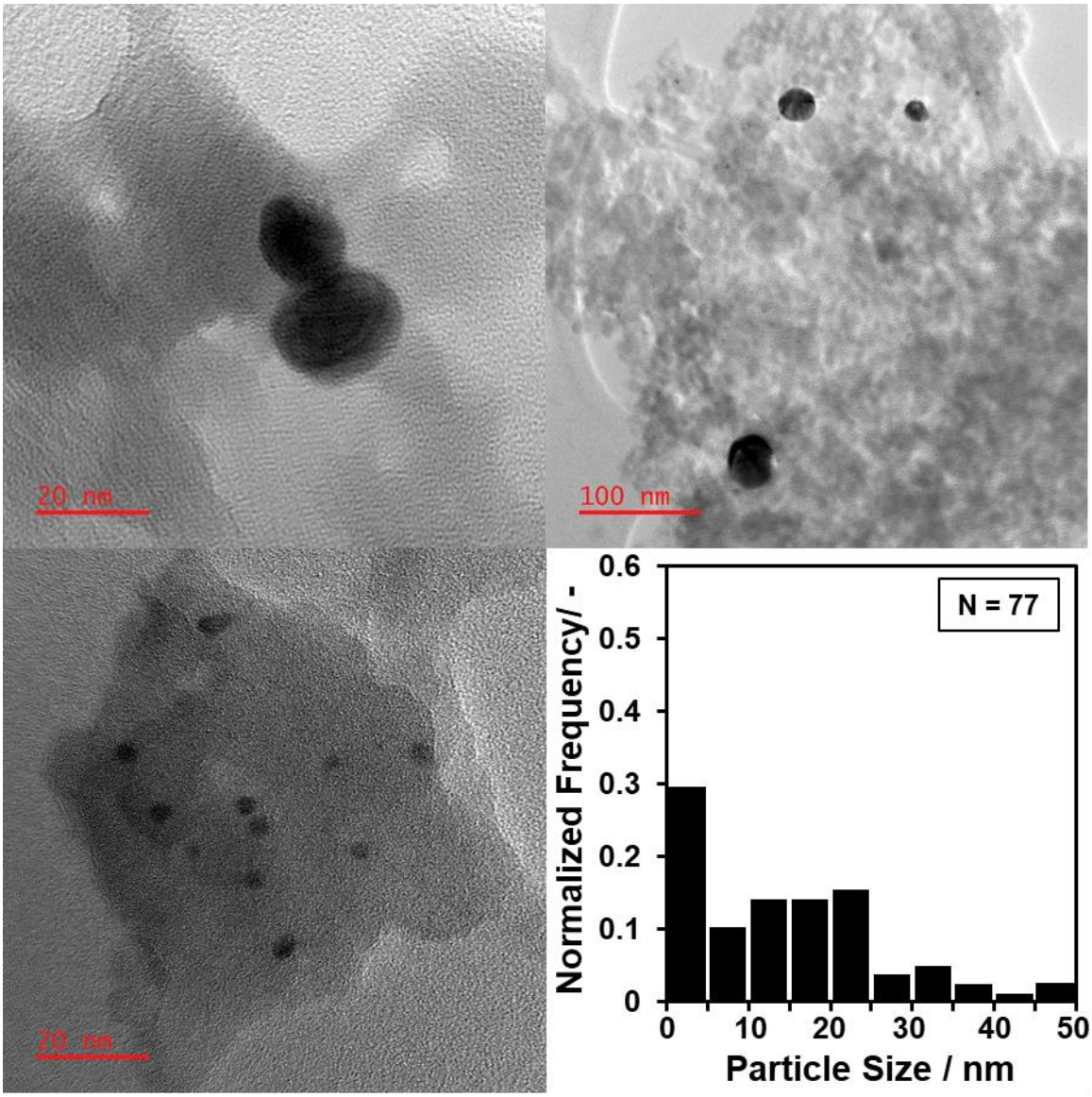

Figure S.9. TEM images and particle size distribution of used Pd/SiO_2. This particle sample was subjected to multiple kinetic experiments at various conditions, approximately 100 hours of time on stream. Average particle size was shown to be 15.1 ± 11.2 nm.

S.6. XRD Data

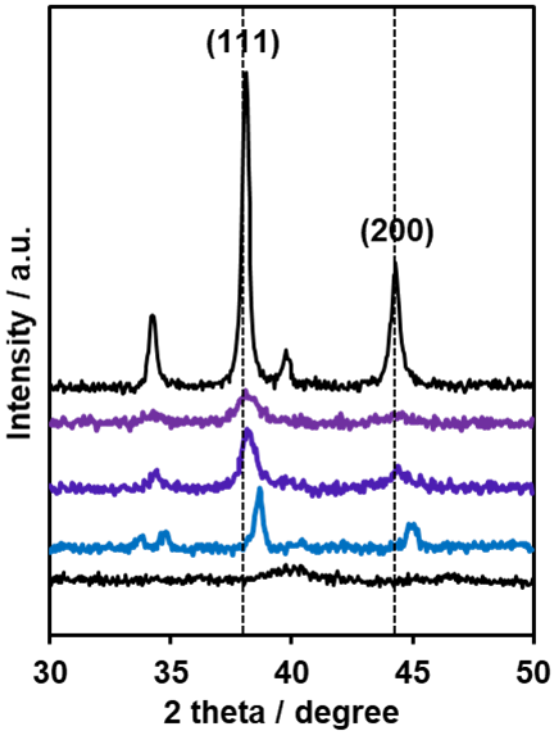

Figure S.10. X-ray diffraction patterns for Au, Pd and PdAu/SiO_2 catalysts. From top to bottom; Au/SiO_2 (black), 1:53 PdAu/SiO_2 (light purple), 1:10 PdAu/SiO_2 (dark purple), 1:2 PdAu/SiO_2 (blue), Pd/SiO_2 (black).

S.7. UV-Vis Data

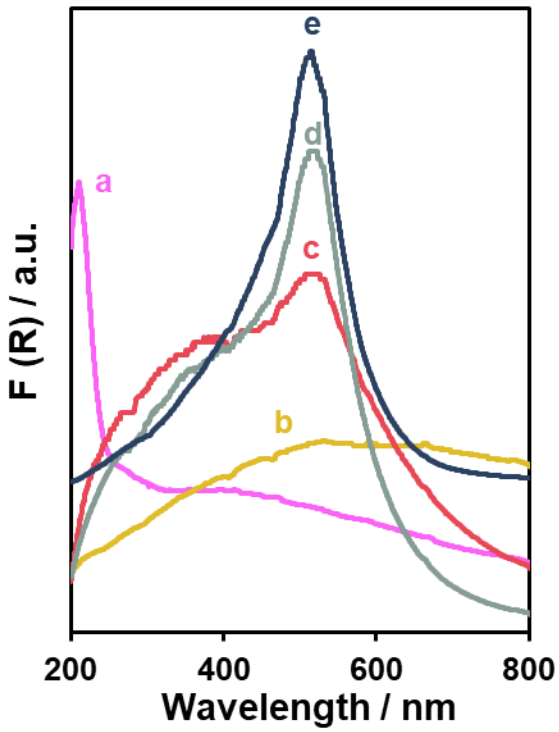

Figure S.11. Diffuse reflectance UV-Visible spectra of catalysts used in this study (a) Pd/SiO_2 (b) 1:2 $PdAu/SiO_2$ (c) 1:10 $PdAu/SiO_2$ (d) 1:53 $PdAu/SiO_2$ (e) Au/SiO_2.

S.8 GradientCheck Calculations

The GradientCheck tool developed by Hickman et al. [10] was used to assess the relevance of heat and mass transfer limitations to the rates observed in this study. A screenshot of the example output files for the highest rates measured in this study are shown in Figure S.7.1. The authors note that GradientCheck does not allow in input of more than two reactants and such cannot accurately reflect all 3 reactants present in this work. For the sake of including the methanol and dimethylamine, the largest and the coupled molecules, oxygen was left out of the calculations. Based on these results, we concluded that heat and mass transfer limitations were likely irrelevant based on the rates measured in this study, and thus the rates reported are limited solely by kinetics and not by diffusion.

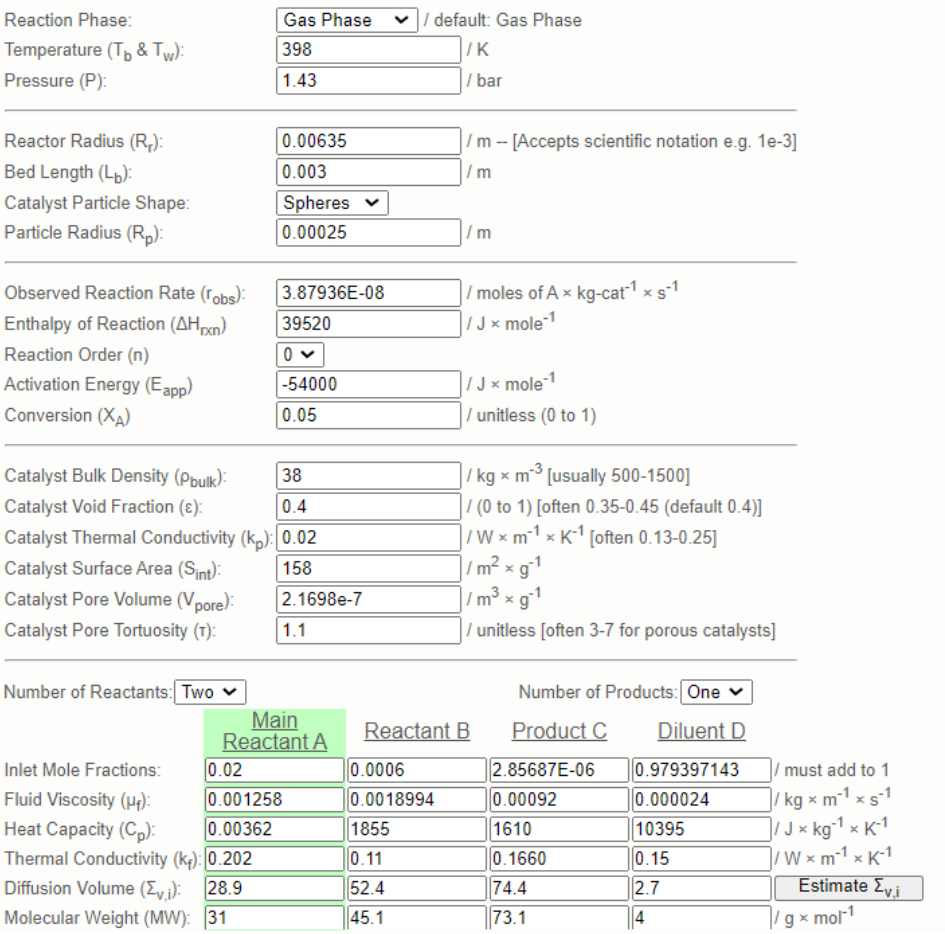

Figure S.12. Inputs for GradientCheck.

$r_{obs} < r_{max}$	no	Is the observed reaction rate realistic?
$\sum y_i = 1$	yes	Do the mole fractions add to one?
$0.25 < \varepsilon < 0.55$	yes	Is the void fraction within typical range?
$0.1 < k_p < 1$	no	Is the particle conductivity within typical range?
$\varepsilon_p < 0.7$	yes	Is the porosity within typical range?
$2 < \tau < 6$	no	Is the tortuosity within typical range?
$0.5 < Pr < 1.5$	no	Is the Prandtl number within typical range for a gas?
$Re_{Liq} > 0.01$ or $Re_{Gas} > 1$	no	Is the Reynolds number within the valid range for j-factor correlations?
$\beta > 0.3$	Undefined	Are multiple steady states possible?
$(C_b - C_s)/C_b > 5\%$	yes!	Does external diffusion limit reaction rate?
$(C_b - C_s)/C_b > 50\%$	yes!	Does external diffusion control reaction rate?
$\lvert T_b - T_s \rvert > 1$ K	Undefined	Is the external temperature gradient significant?
$\lvert T_s - T_c \rvert > 1$ K	Undefined	Is the internal temperature gradient significant?
$\eta < 0.95$	Undefined	Does pore diffusion limit reaction rate?
$\eta < 0.5$	Undefined	Does pore diffusion strongly affect reaction rate?
$\Delta P > 0.2P$	no	Is the bed pressure drop greater than 20% of the total pressure?
+ Mears Axial Dispersion	no	Does axial dispersion have a large effect upon rate?
+ Gierman Axial Dispersion	no	Does axial dispersion have a large effect upon rate?
+ Sie Wall Effects	no	Do broad radial velocity profiles negatively effect the reactant RTD?
+ Mears Radial Interparticle	yes!	Does a radial interparticle heat transport limitation indicate a nonisothermal reactor?

Figure S.13. Results for GradientCheck calculations.

S.9. Methanol Self-coupling Data

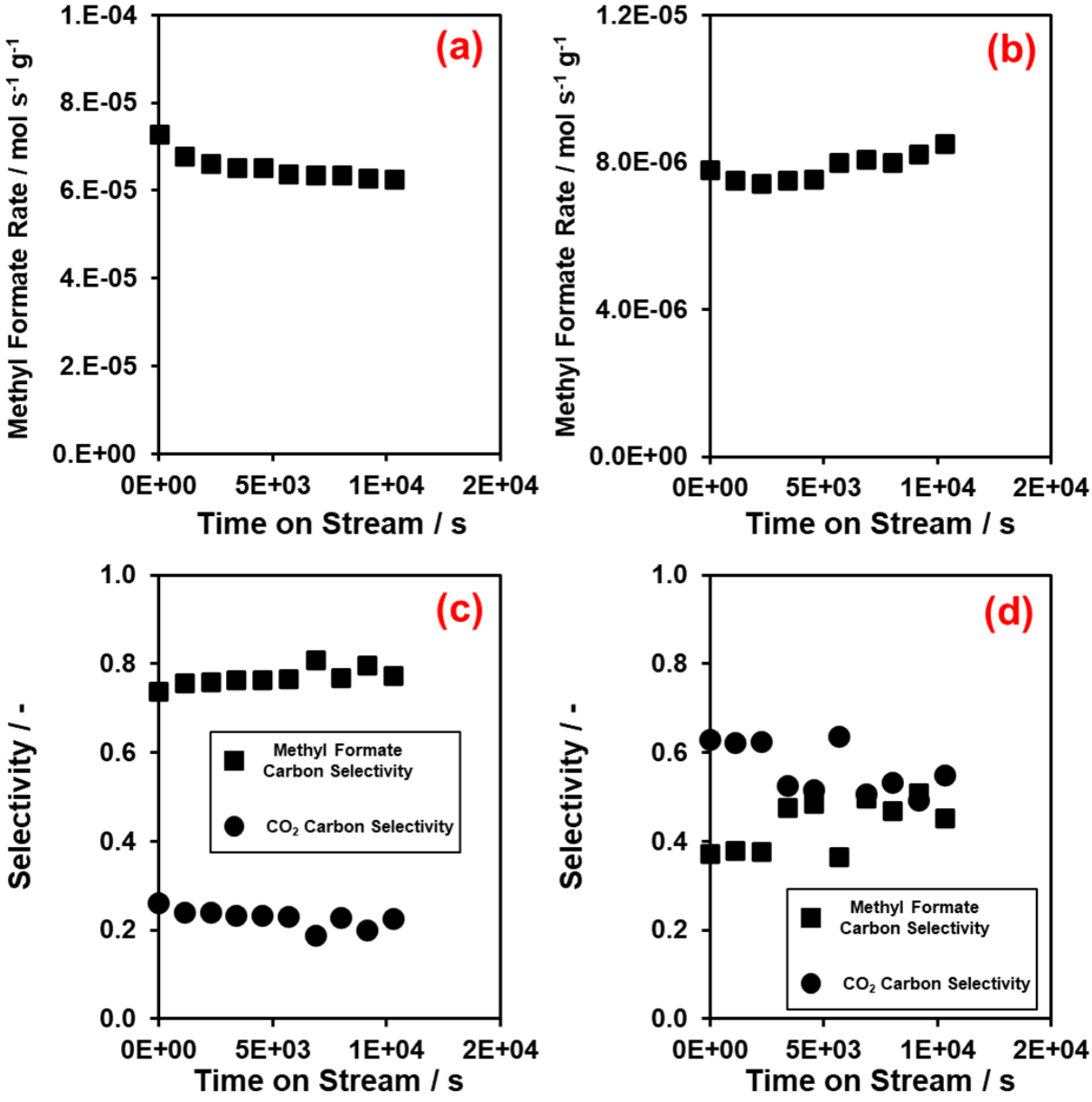

Figure S.14. (a) Time on stream data showing methyl formate production from npAu during gas-phase oxidative self-coupling of methanol. (b) Time on stream data showing methyl formate production from Ag/SiO_2 during gas-phase oxidative self-coupling of methanol. (c) Carbon selectivity of methanol self-coupling during gas-phase oxidative self-coupling of methanol on npAu. (d) Carbon selectivity of methanol self-coupling during gas-phase oxidative self-coupling of methanol on Ag/SiO_2. Reaction Conditions: 143 kPa (2.9 kPa methanol, 1.4 kPa O_2, 1.4 kPa CH_4, , balance He), 448 K, npAu mass: 43.3 mg, Ag/SiO_2 mass: 28.5 mg

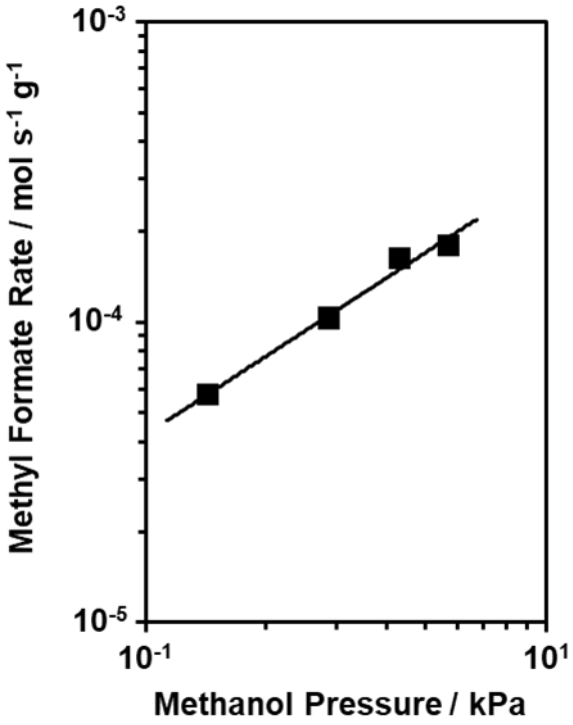

Figure S.15. Methanol reaction order in the oxidative coupling of methanol on npAu. Reaction conditions: 143 kPa (1.4-5.7 kPa methanol, 1.4 kPa O_2, 1.4 kPa CH_4, Balance He), 448K, npAu mass; 43 mg.

S.10 DMF Apparent Activation Energy and Reaction Orders

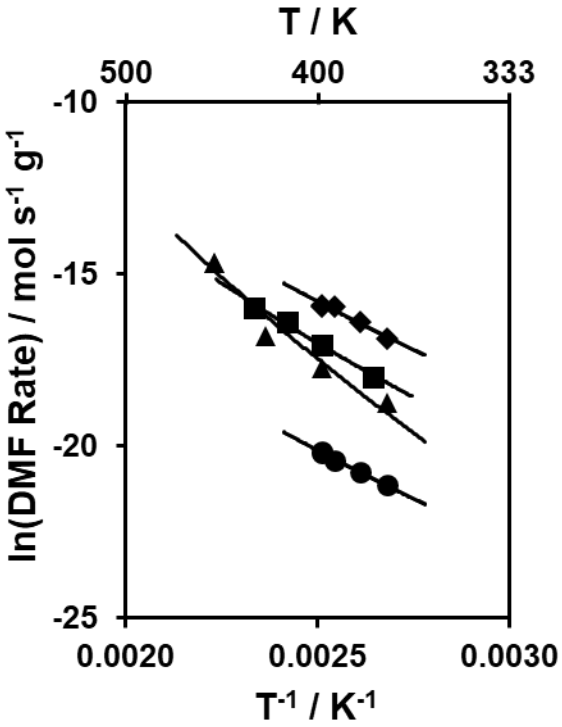

Figure S.16. Arrhenius plots for DMF formation rates over npAu (diamonds), 1:15 $AgAu/SiO_2$ (triangles), Pd/SiO_2 (circles) and 1:10 $PdAu/SiO_2$ (squares). Reaction conditions: 143 kPa total pressure (2.85 kPa methanol, 1.4 kPa O_2, 0.0086 kPa DMA, balance He), 373-448 K, npAu mass ; 12.9 mg (GHSV: 170000 h^{-1}); 1:15 $AgAu/SiO_2$ mass; 6.7 mg (GHSV: 175000 h^{-1}); Pd/SiO_2 mass; 20.1 mg (GHSV: 20700 h^{-1}); 1:10 $PdAu/SiO_2$ mass; 5.4 mg (GHSV: 197000 h^{-1}); each diluted with Si-xerogel.

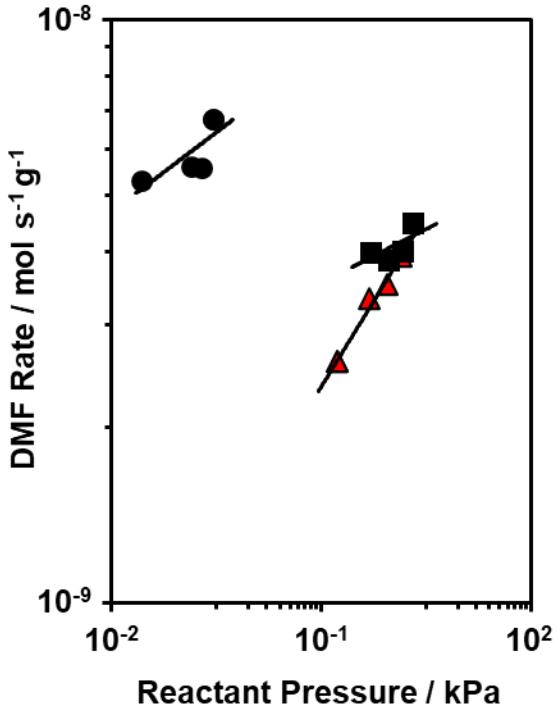

Figure S.17. Reaction orders of DMA (circles), O_2 (red triangles, color to distinguish in data overlap), and methanol (squares). Reaction conditions: 143 kPa (2.9-5.9 kPa methanol, 1.4-4.3 kPa O_2, 0.019-0.094 kPa DMA, Balance He), 398K, npAu mass; 0.029 g (GHSV: 170000 h^{-1}).

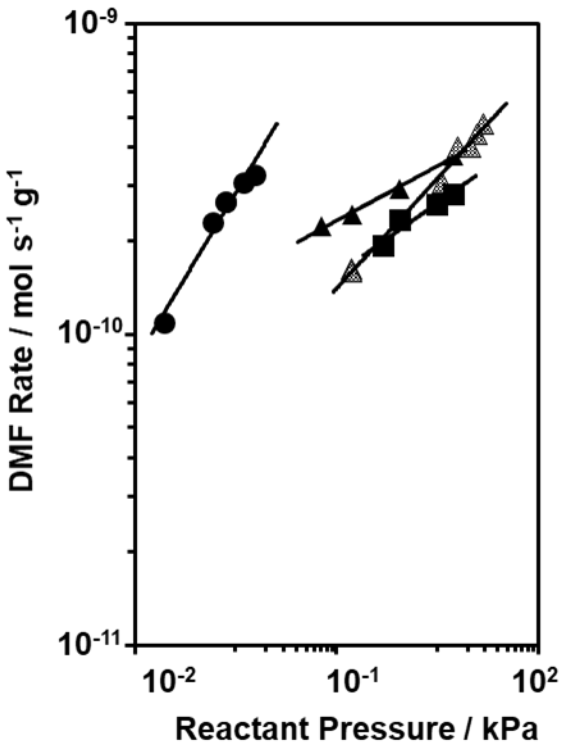

Figure S.18. Reaction orders of DMA (circles), O_2 (triangles; gray at lower O_2 pressures and black at higher O_2 pressures on the same loading of catalyst weeks apart from one another), and methanol (squares). Reaction conditions: 141 kPa (2.85-14.27 kPa methanol, 0.72-28.54 kPa O_2, 0.019-0.156 kPa DMA, Balance He), 398 K, 1:15 $AgAu/SiO_2$ mass; 0.0093 g diluted in in Si-xerogel (approximately twice the catalyst mass) (GHSV: 175000 h^{-1}). Catalyst and Si-xerogel diluent sieved to 180μm-250 μm.

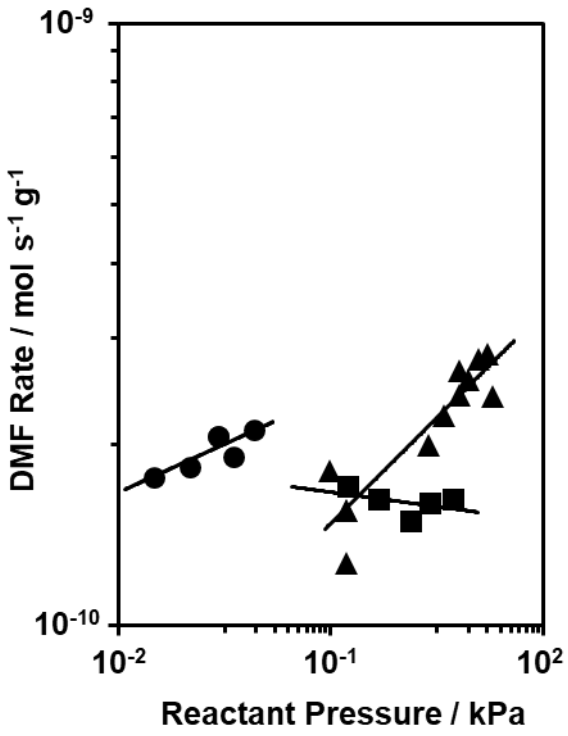

Figure S.19. Reaction orders of DMA (circles), O_2 (triangles), and methanol (squares) over Pd/SiO_2. Reaction conditions: 141 kPa (1.00-5.70 kPa methanol, 1.10-8.56 kPa O_2, 0.014-0.156 kPa DMA, Balance He), 398 K, Pd/SiO_2 mass; 0.0140-0.0201 g diluted in Si-xerogel (approximately equal the catalyst mass) mg (GHSV: 207000 h^{-1}). Catalyst and Si-xerogel diluent sieved to 180μm-250 μm.

S.11. CO_2 Apparent Activation Energy and Reaction Orders

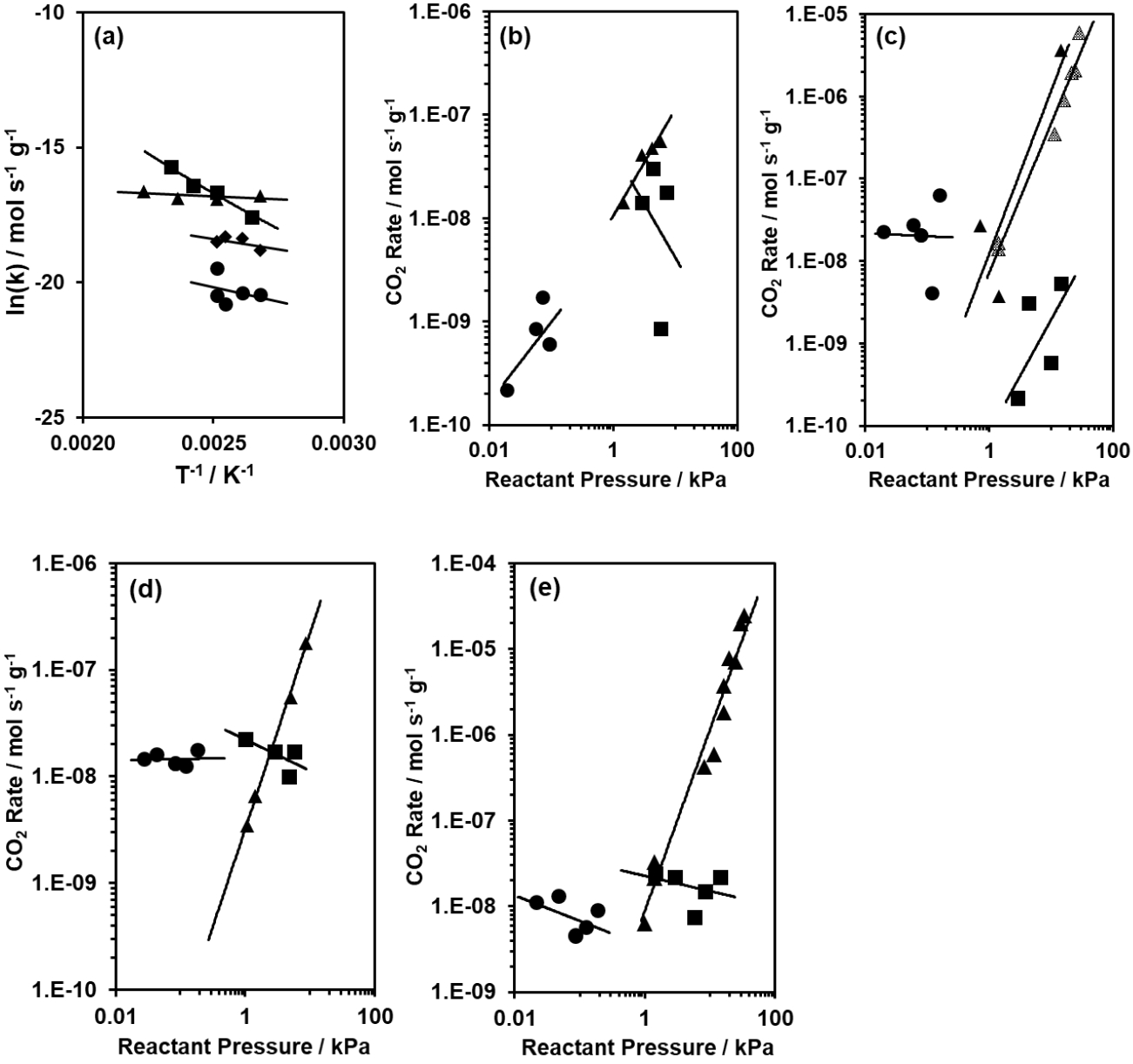

Figure S.20. (a) Arrhenius plots for CO_2 formation rates over npAu (diamonds), 1:15 $AgAu/SiO_2$ (triangles), Pd/SiO_2 (circles) and 1:10 $PdAu/SiO_2$ (squares). Reaction conditions: 143 kPa total pressure (2.85 kPa methanol, 1.4 kPa O_2, 0.0086 kPa DMA, balance He), 373 K-448 K, $AgAu/SiO_2$ mass; 6.7 mg (WHSV: 175000 h^{-1}); Pd/SiO_2 mass; 20.1 mg (WHSV: 207000 h^{-1}); $PdAu/SiO_2$ mass; 5.4 mg (WHSV: 197000 h^{-1}); each diluted with Si-xerogel. (b)-(e) Reaction orders of DMA (circles), O_2 (triangles), and methanol (squares). ((b):npAu, (c):$AgAu/SiO_2$, (d): $PdAu/SiO_2$, (e): Pd/SiO_2). Reaction conditions: 141-143 kPa (1.00-14.27 kPa methanol, 0.72-28.54 kPa O_2, 0.014-0.156 kPa DMA, Balance He), 398K, npAu mass; 0.029 g. 1:15 $AgAu/SiO_2$ mass; 0.0093 g, 1:10 $PdAu/SiO_2$ mass; 0.0054-0.0058 g, Pd/SiO_2 mass; 0.0140-0.0201 g, diluted in in Si-xerogel (approximately twice the catalyst mass). Catalyst and Si-xerogel diluent sieved to 180μm-250μm.

Table S.2. Summary of apparent activation energies and reaction orders of various samples tested in this study.					
Catalyst	**CO_2 Formation E_{app} / kJ mol^{-1}**	**CO_2 reaction orders**			
		CH_3OH	**O_2**	**DMA**	**DMF**
npAu	26 ± 11	-1.04 ± 1.88	1.03 ± 0.15	0.77 ± 0.47	-
1:15 $AgAu/SiO_2$	16 ± 4	1.37 ± 0.85	2.25 ± 0.77	-0.04 ± 0.62	-
Pd/SiO_2	29 ± 31	0.00 ± 0.02	1.88 ± 0.18	0.09 ± 0.04	-
1:10 $PdAu/SiO_2$	63 ± 5	-0.18 ± 0.25	1.39 ± 0.34	-0.30 ± 0.27	-

S.12. Example Transient Data with Long Time on Stream

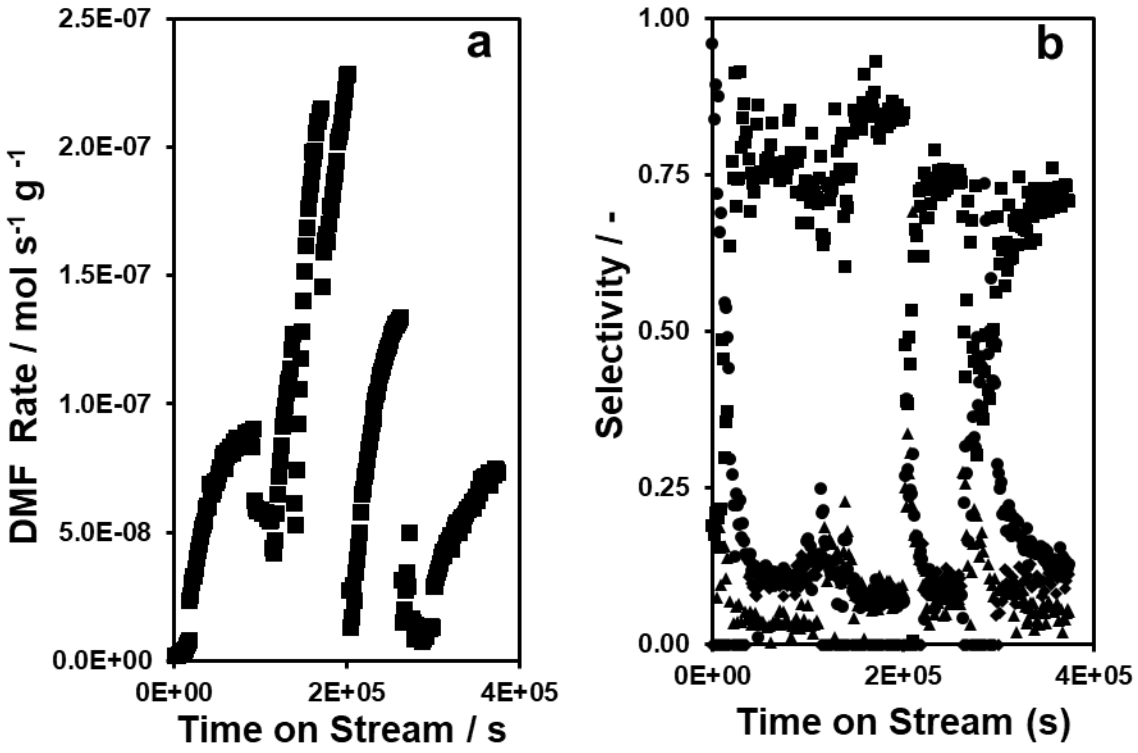

Figure S.21. (a) Long transients observed as a result of methanol and DMA concentration changes. (b) Selectivity during the transients is variable; DMF (squares), CO_2 (circles), formaldehyde (triangles), methyl formate (diamonds). Reaction conditions: 143 kPa (2.9-14.3 kPa methanol, 1.4 kPa O_2, 0.17-0.86 kPa DMA, 1.4 kPa CH_4, Balance He), 448 K, npAu mass: 43.3 mg.

S.13 DMF Co-fed Data

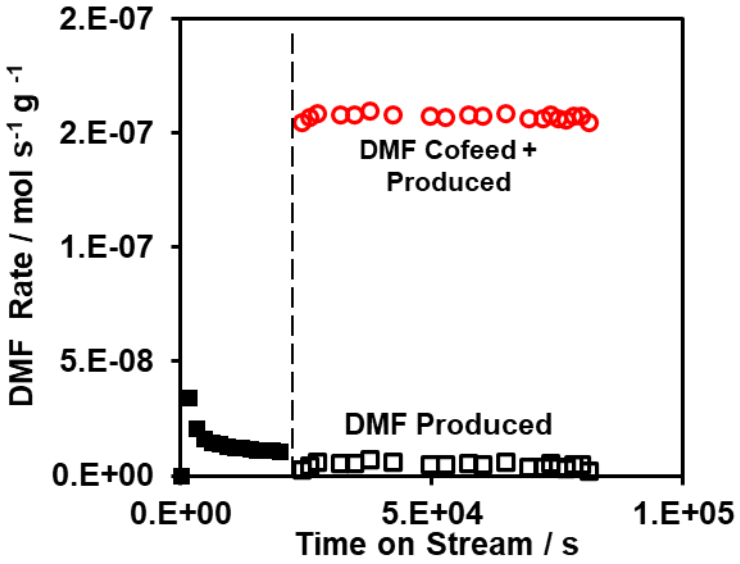

Figure S.22. DMF co-fed off/on. Reaction conditions: 143 kPa (2.9 kPa methanol, 1.4 kPa O_2, 0.065 kPa DMA, 1.4 kPa CH_4, 0.0088 kPa DMF Balance He), 398K, npAu mass; 29 mg.

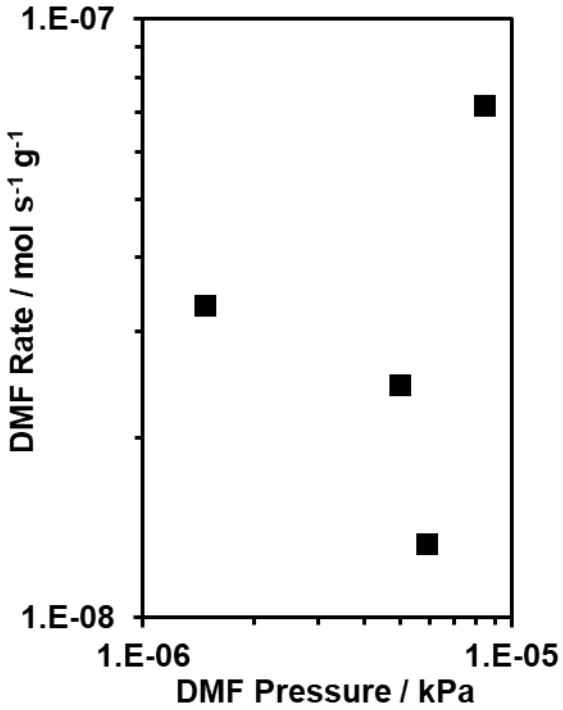

Figure S.23. DMF reaction order on 1:10 PdAu/SiO_2. Reaction conditions: 143 kPa (2.9 kPa methanol, 1.4 kPa O_2, 0.17-0.86 kPa DMA, 1.4 kPa CH_4, 0.00015-0.00084 kPa DMF, balance He), 398 K, 1:8 PdAu/SiO_2 mass: 6.0 mg.

S.14 Pd, PdAu, and PdCu Rate and Selectivity Comparison Data

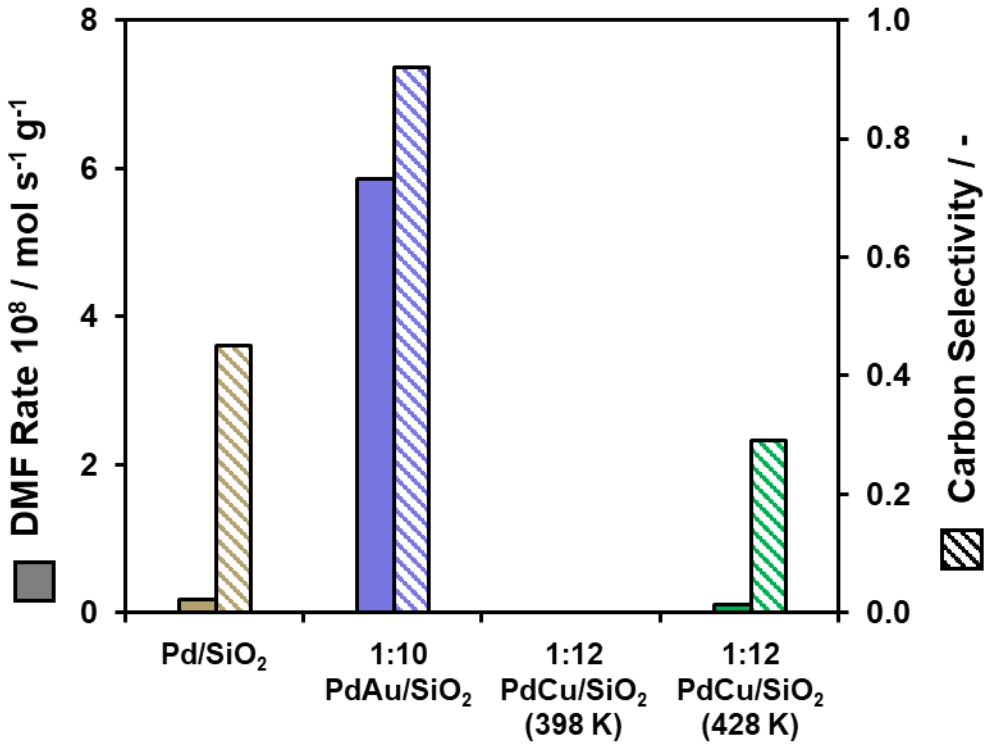

Figure S.24. DMF rate and selectivity of Pd/SiO_2, 1:10 $PdAu/SiO_2$, and 1:15 $PdCu/SiO_2$ with data for 1:12 $PdCu/SiO_2$ being shown at two different temperatures. Reaction Conditions: 141 kPa (2.82 kPa methanol, 1.41 kPa O_2, 0.085 kPa DMA, 0.141 kPa CH_4, Balance He), 398 K and 428 K, Catalyst mass; 0.005-0.015 g diluted in Si-xerogel (approximately twice the catalyst mass). Catalyst and Si-xerogel diluent sieved to 180μm-250μm.

S.15 DFT Computational Inputs

VASP INCAR Files (SI)

INCAR for Surface Calculation

ENAUG = 750.000000
ENCUT = 500.000000
POTIM = 0.200000
SIGMA = 0.200000
EDIFF = 1.00e-08
EDIFFG = -2.00e-02
ALGO = normal
GGA = PE
IBRION = 1
ICHARG = 1
ISIF = 2
ISMEAR = 0
ISTART = 1
ISYM = 0
KPAR = 1
LMAXMIX = 6
LORBIT = 10
NELM = 100
NSW = 0
IVDW = 13
VDW_S6 = 1.000000
VDW_S8 = 0.959481
VDW_A1 = 0.385750
VDW_A2 = 4.806885
NCORE = 2
LASPH = .TRUE.
LCHARG = .FALSE.
LWAVE = .FALSE.
LREAL = .FALSE.
IDIPOL= 3
LDIPOL= .TRUE.

INCAR for Hessian Calculation

ENAUG = 750.000000
ENCUT = 500.000000
POTIM = 0.0050000
SIGMA = 0.200000
EDIFF = 1.00e-08
ALGO = normal
GGA = PE
IBRION = 5
NFREE = 4
ICHARG = 1
ISIF = 2
ISMEAR = 0
ISTART = 1
ISYM = 0

KPAR = 1
LMAXMIX = 6
LORBIT = 10
NELM = 100
NSW = 0
IVDW = 13
VDW_S6 = 1.000000
VDW_S8 = 0.959481
VDW_A1 = 0.385750
VDW_A2 = 4.806885
NCORE = 2
LASPH = .TRUE.
LCHARG = .FALSE.
LWAVE = .FALSE.
LREAL = .FALSE.
IDIPOL= 3
LDIPOL= .TRUE.

VASP POTCAR Files (SI)

Au	PAW_PBE Au 04Oct2007
Pd	PAW_PBE Pd 04Jan2005
Ag	PAW_PBE Ag 02Apr2005
O	PAW_PBE O 08Apr2002
C	PAW_PBE C 08Apr2002
H	PAW_PBE H 15Jun2001
N	PAW_PBE N 08Apr2002

VASP KPOINTS Files (SI)

KPOINTS for Bulk Calculations
0
Gamma
15 15 15
0 0 0

KPOINTS for Surface Calculations
0
Gamma
5 5 1
0 0 0

S.16 References

1. Y. Xu and M. Mavrikakis, *J. Phys. Chem. B*, 2003, **107**, 9298-9307.
2. J. Kim, E. Samano and B. E. Koel, *Surface Science*, 2006, **600**, 4622-4632.
3. J. L. C. Fajín, M. N. D. S. Cordeiro and J. R. B. Gomes, *The Journal of Physical Chemistry C*, 2007, **111**, 17311-17321.
4. L. C. Wang, M. L. Personick, S. Karakalos, R. Fushimi, C. M. Friend and R. J. Madix, *Journal of Catalysis*, 2016, **344**, 778-783.
5. C. T. Campbell, *Surface Science*, 1985, **157**, 43-60.
6. M. Gajdoš, A. Eichler and J. Hafner, *Surface Science*, 2003, **531**, 272-286.
7. M. Yan, Z.-Q. Huang, Y. Zhang and C.-R. Chang, *Phys. Chem. Chem. Phys.*, 2017, **19**, 2364-2371.
8. P. Junell, K. Honkala, M. Hirsimäki, M. Valden and K. Lassonen, *Surface Science*, 2003, **546**, L797-L802.
9. D.-J. Liu and J. W. Evans, *Phys. Rev. B*, 2014, **89**, 205406.
10. D. A. Hickman, J. C. Degenstein and F. H. Ribeiro, *Current Opinion in Chemical Engineering*, 2016, **13**, 1-9.